Synthesis and Copper Coordination Chemistry of Hindered 1,4,7-Triazacyclononane Ligands with Amide Appendages

Lisa M. Berreau, Jason A. Halfen, Victor G. Young, Jr., and William B. Tolman*

Department of Chemistry and Center for Metals in Biocatalysis, University of Minnesota, 207 Pleasant Street SE, Minneapolis, Minnesota 55455

Received August 29, 1997

Copper complexes of the new ligands[1a] L^{Piv} and $L^{RAmR'}$ that comprise 1,4-diisopropyl-1,4,7-triazacyclononanes linked to secondary and tertiary amide groups were prepared and characterized, with a particular view toward evaluating amide structural, spectroscopic, and potential hydrogen-bonding influences of relevance to ongoing copper−dioxygen reactivity studies. X-ray crystal structures of the Cu(I) complexes [LCu(CH_3CN)]X (L = L^{HAmMe}, X = ClO_4; L = L^{Piv}, X = CF_3SO_3) revealed typical 4-coordinate geometries with the amide dangling free, while those of the Cu(II) compounds [LCuCl]X (L = L^{HAmMe}, X = ClO_4; L = L^{MeAmH}, X = PF_6) and [L^{Piv}Cu(O_3SCF_3)]O_3SCF_3 showed 5-coordinate square pyramidal geometries with the amide coordinated to the metal via its carbonyl oxygen atom. Analysis of FTIR spectra of the aforementioned compounds and the carbon monoxide adducts [$L^{MeAmR'}$Cu(CO)]SbF_6 (R′ = H or Me) allowed (i) identification of signatures of amide structural features, hydrogen bonding, and metal coordination and (ii) classification of the amide ligands as generally electron withdrawing relative to alkyl-substituted counterparts (e.g., 1,4,7-triisopropyl-1,4,7-triazacyclononane).

Hydrogen-bonding interactions have long been recognized to influence the chemistry of iron−dioxygen adducts in the active sites of heme proteins, the classic example being the oxy form of hemoglobin, in which hydrogen bonding between a distal hystidyl proton and the end-on-bound superoxide moiety plays a key stabilizing role.[1b,2] Hydrogen bonds also may influence the process of dioxygen activation, as exemplified by the proposed involvement of distal H-bonding in promoting O−O bond heterolysis[3] and in controlling the reactivity of the subsequently generated ferryl unit during the catalytic mechanism traversed by the heme-iron enzymes catalase and peroxidase.[4] Important insights into the influence of these hydrogen-bonding interactions have emerged from synthetic modeling studies wherein the dioxygen-binding properties of iron complexes of various porphyrins with H-bond donor amide groups have been examined.[5]

Active-site hydrogen bonds to biological metal−dioxygen species probably also are important in nonheme systems, although less is known about these compared to the well-studied heme cases. The best characterized example is the oxy form of the reversible O_2 carrier hemerythrin that is stabilized by H-bonding between the η^1-hydroperoxide and the oxo ligand that bridges the two iron(III) atoms.[6] H-bonding also has been proposed to be important in dioxygen activation mechanisms in some nonheme enzymes (cf. dopamine β-monooxygenase, DβM)[7] and may be readily envisaged to play a central role in O_2 activation pathways in many others for which our understanding of mechanism is just evolving.[8] Conclusive evidence of H-bonding in biomimetic non-porphyrin metal−dioxygen complexes is scarce, however. One example is the observation of isomeric forms of a monomeric manganese peroxo species that differ only with respect to the absence or presence of an intramolecular H-bond between the peroxo ligand and a nearby bound pyrazole.[9] More recently, a mononuclear copper−hydroperoxo complex stabilized by H-bonding between ligand amide groups and the −OOH unit was reported.[10] However, a proposed[11a] monocopper−superoxo complex supported by an array of H-bonds with a similar amide-containing ligand was found instead to be a copper−hydroxide species.[11b]

(1) (a) Abbreviations used: TACN = 1,4,7-triazacyclononane, L^{Bn_3} = 1,4,7-tribenzyl-1,4,7-triazacyclononane. For remaining macrocycles, L = 1,4-diisopropyl-7-X-1,4,7-triazacyclononane, where for L^{iPr_3}, X = isopropyl, for L^{iPr_2Bn}, X = benzyl, for L^{H}, X = H, for L^{HAmH}, X = *tert*-butylacetamido, for L^{HAmMe}, X = *tert*-butyl-*N*-methylacetamido, for L^{MeAmH}, X = *tert*-butyl-2-propionamido, for L^{MeAmMe}, X = *N*-methyl-*N*-*tert*-butyl-2-propionamido, and for L^{Piv}, X = 2-pivalamidoethyl. (b) Pauling, L. *Nature* **1964**, *203*, 182−183.

(2) Springer, B. A.; Sligar, S. G.; Olson, J. S.; Phillips, G. N., Jr. *Chem. Rev.* **1994**, *94*, 699−714.

(3) (a) Poulos, T. L. *Adv. Inorg. Biochem.* **1988**, *7*, 1−36. (b) Dawson, J. H. *Science* **1988**, *240*, 433−439. (c) Gerber, N. C.; Sligar, S. G. *J. Am. Chem. Soc.* **1992**, *114*, 8742−8743 and references therein.

(4) (a) Kitagawa, T.; Mizutani, Y. *Coord. Chem. Rev.* **1994**, *135*, 685−735. (b) Mukai, M.; Nagano, S.; Tanaka, M.; Ishimori, K.; Morishima, I.; Ogura, T.; Watanabe, Y.; Kitagawa, T. *J. Am. Chem. Soc.* **1997**, *119*, 1758−1766 and references therein.

(5) (a) Momenteau, M.; Reed, C. A. *Chem. Rev.* **1994**, *94*, 659−698. (b) Wuenschell, G. E.; Tetreau, C.; Lavalette, D.; Reed, C. A. *J. Am. Chem. Soc.* **1992**, *114*, 3346−3355. (c) Chang, C. K.; Liang, Y.; Avilés, F. *J. Am. Chem. Soc.* **1995**, *117*, 4191−4192. (d) Collman, J. P.; Zhang, X.; Wong, K.; Brauman, J. I. *J. Am. Chem. Soc.* **1994**, *116*, 6245−6251.

(6) (a) Stenkamp, R. E. *Chem. Rev.* **1994**, *94*, 715−726. (b) Shiemke, A. K.; Loehr, T. M.; Sanders-Loehr, J. *J. Am. Chem. Soc.* **1986**, *108*, 2437−2443.

(7) Tian, G.; Berry, J. A.; Klinman, J. P. *Biochemistry* **1994**, *33*, 226−234.

(8) For examples, see: (a) Klinman, J. P. *Chem. Rev.* **1996**, *96*, 2541−2561. (b) Solomon, E. I.; Sundaram, U. M.; Machonkin, T. E. *Chem. Rev.* **1996**, *96*, 2563−2605. (c) Feig, A. L.; Lippard, S. J. *Chem. Rev.* **1994**, *94*, 759−805. (d) Wallar, B. J.; Lipscomb, J. D. *Chem. Rev.* **1996**, *96*, 2625−2657.

(9) Kitajima, N.; Komatsuzaki, H.; Hikichi, S.; Osawa, M.; Moro-oka, Y. *J. Am. Chem. Soc.* **1994**, *116*, 11596−11597.

(10) Wada, A.; Harata, M.; Hasegawa, K.; Jitsukawa, K.; Masuda, H.; Einaga, H. *J. Inorg. Biochem.* **1997**, *67*, 73.

S0020-1669(97)01115-4 CCC: $15.00
Published on Web 02/11/1998

Inspired by the previous successes in modeling protein active−site H-bonding interactions in heme-iron/dioxygen adducts through the use of amide-functionalized porphyrins and the probable importance of analogous interactions in various non-heme systems, we have initiated research aimed at defining the influence of potential H-bond donor functional groups on the dioxygen activation chemistry of synthetic, non-porphyrin complexes. We showed previously that isomeric (μ-η^2:η^2-peroxo)- and bis(μ-oxo)dicopper cores could be generated upon reaction of dioxygen with Cu(I) complexes of sterically hindered 1,4,7-trialkyl-substituted 1,4,7-triazacyclononane (TACN) ligands at low temperature.[12] The nature of the alkyl substituents was found to influence the course of the oxygenation chemistry, the interconvertibility of the two isomeric cores, and their C−H bond activation (monooxygenase-modeling) reactivity. To address the possible effects of H-bonding on these and other issues, we have targeted a family of amide-functionalized derivatives of the TACN framework for synthesis and systematic study, beginning for the sake of simplicity with ligands that have a single amide arm.[13] Investigation of the degradation of copper−dioxygen complexes of these ligands also may allow us to probe amide oxidation akin to that performed by the copper-containing peptidylglycine α-amidating monooxygenase.[8a,14]

In this contribution we describe results obtained during the initial phase of the project involving the preparation and characterization of a set of such new ligands and some of their representative Cu(I) and Cu(II) complexes. This work was undertaken with a specific view toward elucidating the structural and spectroscopic features that arise from the presence of the various different amide appendages.[15] These features are relevant to interesting influences of these amide arms on the dioxygen chemistry of the Cu(I) compounds and their subsequent oxidative degradation that we have uncovered (to be reported separately[16]).

Results and Discussion

Synthesis of Ligands and Complexes. We prepared two types of mono-amide-functionalized ligands, L^{Piv} and $L^{RAmR'}$ (Scheme 1), that differ with respect to the orientation of the amide unit (carbonyl "outside" vs "inside", respectively) and the length of the tether connecting the amide group to the TACN frame (two- vs one-carbon chain, respectively). Four variants of the $L^{RAmR'}$ class were targeted, our reasoning being that (i) comparison of the properties of complexes of ligands with secondary (R′ = H) and tertiary (R′ = alkyl) amides would help us identify H-bonding interactions for the former and (ii) by changing R, we would be able to influence through steric effects the ultimate generation of peroxo- or bis(oxo)dicopper cores. As shown in Scheme 1, all of the ligands were synthesized by suitably derivatizing 1,4-diisopropyl-1,4,7-triazacyclononane (L^H), either by direct means with the appropriate *N-tert*-butyl-*N*-R′-2-haloacetamide or -propionamide[17] to generate the $L^{RAmR'}$ class or through a stepwise sequence to afford L^{Piv}.[18]

Scheme 1

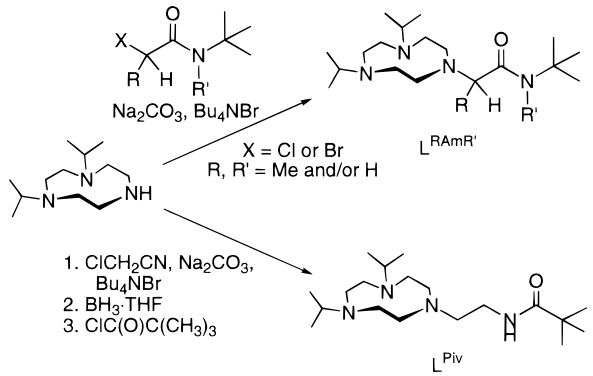

Chart 1

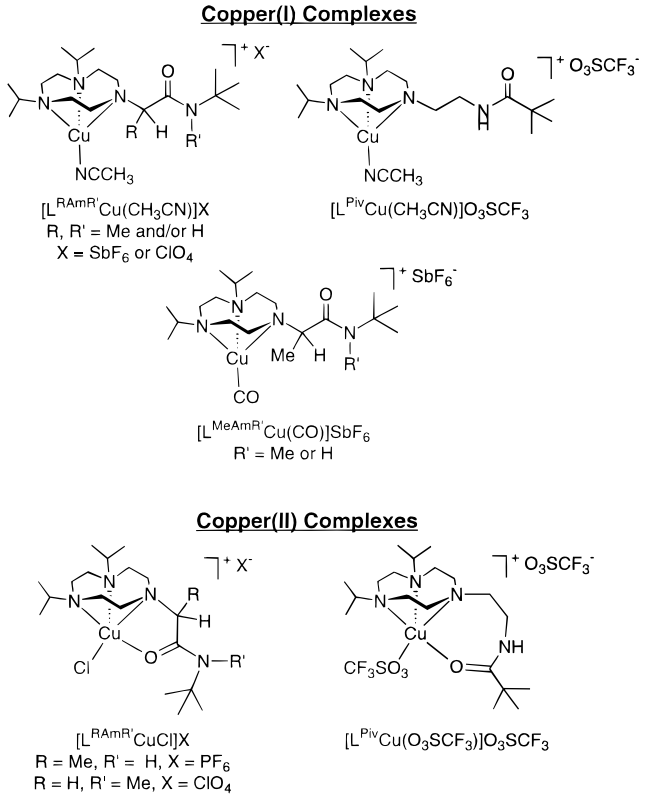

Cu(I) complexes were prepared by treating the ligands with $[Cu(CH_3CN)_4]X$ (X = SbF_6, ClO_4, or O_3SCF_3) in CH_3CN or CH_2Cl_2 under an inert atmosphere (Chart 1). Carbonyl adducts of the compounds ligated by $L^{MeAmR'}$ (R′ = H or Me) were synthesized by treatment of the respective CH_3CN complexes

(11) (a) Harata, M.; Jitsukawa, K.; Masuda, H.; Einaga, H. *J. Am. Chem. Soc.* **1994**, *116*, 10817−10818. (b) Berreau, L. M.; Mahapatra, S.; Halfen, J. A.; Young, V. G., Jr.; Tolman, W. B. *Inorg. Chem.* **1996**, *35*, 6339−6342.

(12) Tolman, W. B. *Acc. Chem. Res.* **1997**, *30*, 227−237.

(13) A copper(II) complex of a tris(peptidyl)-substituted TACN ligand was recently reported: Watson, A. A.; Willis, A. C.; Fairlie, D. P. *Inorg. Chem.* **1997**, *36*, 752−753.

(14) Similar approaches involving examination of the dioxygen reactivity of copper(I) complexes of ligands with amide substituents have been taken. See ref 11 and: (a) Amadéi, E.; Alilou, E. H.; Eydoux, F.; Pierrot, M.; Réglier, M.; Waegell, B. *J. Chem. Soc., Chem. Commun.* **1992**, 1782−1784. (b) Réglier, M.; Amadéi, E.; Alilou, E. H.; Eydoux, F.; Pierrot, M.; Waegell, B. In *Bioinorganic Chemistry of Copper*; Karlin, K. D., Tyeklár, Z., Eds.; Chapman & Hall: New York, 1993; pp 348−362.

(15) Copper complexes of other ligand types with amide appendages have been reported. See ref 13 and: (a) Alilou, E. H.; Amadéi, E.; Giorgi, M.; Pierrot, M.; Réglier, M. *J. Chem. Soc., Dalton Trans.* **1993**, 549−557. (b) Sigel, H.; Martin, R. B. *Chem. Rev.* **1982**, *82*, 385−426. (c) Okuno, T.; Ohba, S.; Nishida, Y. *J. Inorg. Biochem.* **1997**, *67*, 63.

(16) Berreau, L. M.; Que, L., Jr.; Tolman, W. B. Manuscript in preparation.

(17) (a) Speziale, A. J.; Hamm, P. C. *J. Am. Chem. Soc.* **1955**, *78*, 2556−2559. (b) Lowe, J. A.; Hageman, D. L.; Drozda, S. E.; McLean, S.; Bryce, D. K.; Crawford, R. T.; Zorn, S.; Morrone, J.; Bordner, J. *J. Med. Chem.* **1994**, *37*, 3789−3811.

(18) (a) Kruijtzer, J. A. W.; Lefeber, D. J.; Liskamp, R. M. J. *Tetrahedron Lett.* **1997**, *38*, 5335−5338. (b) Fortier, D. G.; McAuley, A. *J. Chem. Soc., Dalton Trans.* **1991**, 101−109.

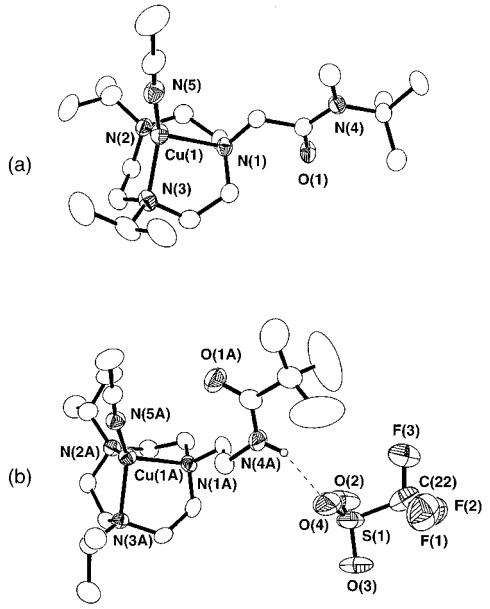

Figure 1. Representations of the X-ray crystal structures of (a) the cationic portion of $[L^{HAmMe}Cu(CH_3CN)]ClO_4$ and (b) $[L^{Piv}Cu(CH_3CN)]O_3SCF_3$ showing non-hydrogen atoms (with the exception of the amide N−H proton of L^{Piv} in structure b) as 50% thermal ellipsoids.

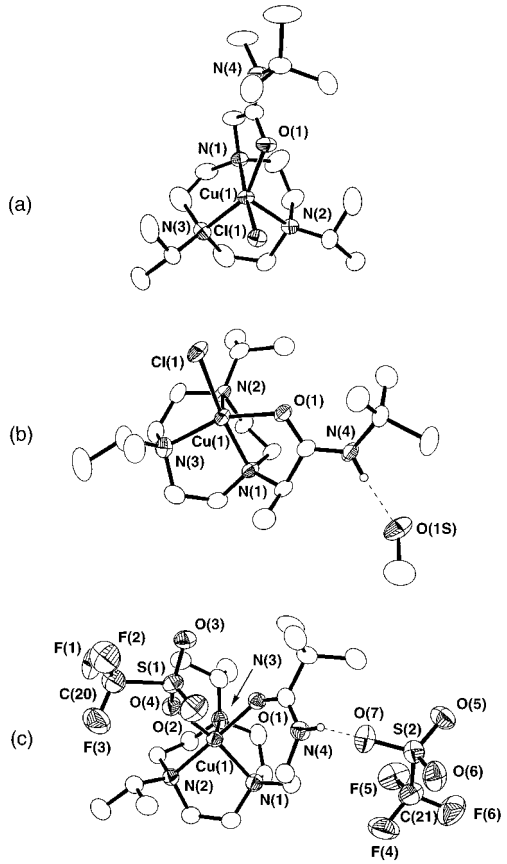

Figure 2. Representations of the X-ray crystal structures of (a) the cationic portion of $[L^{HAmMe}CuCl]ClO_4$, (b) the cationic portion and hydrogen-bonded methanol solvent molecule of $[L^{MeAmH}CuCl]PF_6$·MeOH, and (c) $[L^{Piv}Cu(O_3SCF_3)]O_3SCF_3$ showing non-hydrogen atoms (with the exception of amide N−H protons) as 50% thermal ellipsoids.

with 1 atm of CO. In each instance, the complexes were isolated as air-sensitive crystalline solids and were characterized by CHN analysis, FTIR and NMR spectroscopy, and, in selected instances, X-ray crystallography. Three Cu(II) complexes also were prepared, either via admixture of $L^{RAmR'}$ and $CuCl_2$ followed by anion exchange to yield $[L^{RAmR'}CuCl]X$ (L^{HAmMe}, $X = ClO_4$; L^{MeAmH}, $X = PF_6$) or via treatment of L^{Piv} with $Cu(O_3SCF_3)_2$ to afford $[L^{Piv}Cu(O_3SCF_3)]O_3SCF_3$ (Chart 1). These compounds were characterized by CHN analysis, electrospray MS, X-ray crystallography, and EPR, FTIR, and UV−visible spectroscopy.

X-ray Crystal Structures. Drawings of the crystallographically determined structures of the Cu(I) compounds $[LCu(CH_3CN)]X$ ($L = L^{HAmMe}$, $X = ClO_4$; $L = L^{Piv}$, $X = CF_3SO_3$) are shown in Figure 1, while those of the Cu(II) complexes $[L^{HAmMe}CuCl]ClO_4$, $[L^{MeAmH}CuCl]PF_6$·MeOH, and $[L^{Piv}Cu(O_3SCF_3)]O_3SCF_3$ are shown in Figure 2. The structure of $[L^{MeAmMe}Cu(CH_3CN)]SbF_6$ was also determined but is not described here due to its close similarity to that of $[L^{HAmMe}Cu(CH_3CN)]ClO_4$. Crystallographic data and selected bond distances and angles are listed in Tables 1 and 2, respectively. Complete data for these structures are provided in the Supporting Information.

The Cu(I) complexes adopt slightly distorted C_{3v} geometries such as those of other reported Cu(I) complexes of TACN ligands (Figure 1).[19] As seen previously, the principal distortion from idealized tetrahedral local symmetry involves (i) intraligand N−Cu−N bond angles significantly smaller than those between macrocycle N atoms and the fourth nitrile nitrogen donor [cf. for the L^{HAmMe} structure, average $N_{TACN}-Cu-N_{TACN} = 85°$ vs average $N_{TACN}-Cu-N_{CH_3CN} = 128°$] and (ii) similar $Cu-N_{TACN}$ bond distances (average 2.15 Å) that are significantly longer than the $Cu-NCCH_3$ bond (average 1.86 Å). In all cases, the amide group is planar (<0.06 Å deviation from planarity) and is observed solely in a trans conformation. Importantly, the amide is well-removed from the metal ion and there is no indication of a bonding interaction between the amide and the Cu(I) center in any of these structures. This contrasts with the suggested coordination of an amide carbonyl oxygen in Cu(I) complexes of amide-appended bis[2-(2-pyridyl)ethyl]amine ligands.[15a] In the case of the complex of L^{Piv}, the trifluoromethansulfonate counterion weakly interacts with the substituent amide N−H, as indicated by the N(4)···O(3A) distance of 3.09 Å (the H atom shown was not located; it was placed at an ideal position and refined as a riding atom).

Five-coordinate structures with a bound exogenous Cl^- or $CF_3SO_3^-$ are adopted in the three Cu(II) complexes shown in Figure 2. The amide carbonyl oxygen is coordinated to the metal ion in each structure (average Cu−O = 1.99 Å; range 1.98−2.01 Å), in contrast to the Cu(I) cases but similar to other reported structures of Cu(II) complexes of amide-appended ligands in which the amide group is not deprotonated.[13,15] Geometries somewhat distorted from square pyramidal are apparent from the observed τ values between 0.32 and 0.36 (values of 0 and 1 are indicative of idealized square pyramidal and trigonal bipyramidal geometries, respectively).[20] The coordination geometries of the chloride complexes are quite similar to each other, despite the differences in the nature of the amide arms in the two compounds. Hydrogen bonding to the secondary amide H is seen in the appropriate instances, either to a MeOH solvate (Figure 2a) or to a $CF_3SO_3^-$ counterion (Figure 2c). In the former case, the relevant N(4)···O(1S) distance is 2.85 Å and the hydrogen atom was located in the

(19) (a) Halfen, J. A.; Mahapatra, S.; Wilkinson, E. C.; Gengenbach, A. J.; Young, V. G., Jr.; Que, L., Jr.; Tolman, W. B. *J. Am. Chem. Soc.* **1996**, *118*, 763−776. (b) Chaudhuri, P.; Oder, K. *J. Organomet. Chem.* **1989**, *367*, 249−258.

(20) Addison, A. W.; Rao, T. N.; Reedijk, J.; von Rijn, J.; Verschoor, G. C. *J. Chem. Soc., Dalton Trans.* **1984**, 1349−1356.

Table 1. Summary of X-ray Crystallographic Data[a]

	$[L^{HAmMe}Cu(CH_3CN)]ClO_4$	$[L^{Piv}Cu(CH_3CN)]O_3SCF_3$	$[L^{HAmMe}CuCl]ClO_4$	$[L^{MeAmH}CuCl]PF_6\cdot$ MeOH	$[L^{Piv}Cu(O_3SCF_3)]O_3SCF_3$
empirical formula	$C_{21}H_{43}N_5O_5ClCu$	$C_{22}H_{43}N_5O_4F_3SCu$	$C_{19}H_{40}N_4O_5Cl_2Cu$	$C_{20}H_{44}N_4O_2ClF_6PCu$	$C_{21}H_{40}N_4O_7F_6S_2Cu$
formula weight	544.59	594.21	538.99	616.55	702.23
crystal system	orthorhombic	monoclinic	monoclinic	monoclinic	trigonal
space group	*Pbca*	$P2_1/c$	$P2_1/n$	$P2_1/c$	$R\bar{3}$
a (Å)	15.0617(5)	19.7935(1)	8.0030(1)	8.1388(2)	39.7028(4)
b (Å)	18.2953(6)	10.1110(2)	25.8547(3)	31.3786(4)	39.7028(4)
c (Å)	19.7456(6)	29.0220(5)	12.8547(2)	11.5194(2)	10.4657(2)
α (deg)					
β (deg)		91.345(1)	106.834(1)	103.095(1)	
γ (deg)					
V (Å^3)	5441.1(3)	5806.6(2)	2545.85(6)	2865.37(9)	14287.0(3)
Z	8	8	4	4	18
density (calcd), g cm^{-3}	1.330	1.359	1.406	1.429	1.469
temp (K)	173(2)	173(2)	173(2)	173(2)	173(2)
crystal size (mm)	0.45 × 0.42 × 0.25	0.55 × 0.35 × 0.18	0.50 × 0.28 × 0.25	0.35 × 0.23 × 0.08	0.40 × 0.30 × 0.25
diffractometer	Siemens SMART	Siemens SMART	Siemens SMART	Siemens SMART	Siemens SMART
abs coeff (mm^{-1})	0.939	0.878	1.103	0.974	0.898
2θ max (deg)	50.04	50.06	50.06	50.08	50.02
no. of reflns collected	25 090	27 191	12 665	13 998	24 375
no. of indep reflns	4788	10 086	4489	5036	5596
no. of variable params	388	758	328	404	417
R1/wR2[b]	0.0607/0.1324	0.0739/0.1492	0.0499/0.1151	0.0482/0.0926	0.0482/0.1087
goodness-of-fit (F^2)	1.064	1.023	1.031	1.030	1.147
largest diff features (e Å^{-3})	1.015/−0.550	0.919/−0.490	1.228/−0.487	0.475/−0.334	0.877/−0.349

[a] Radiation used: Mo Kα ($\lambda = 0.710\ 73$ Å). [b] $R1 = \sum||F_o| - |F_c||/\sum|F_o|$; $wR2 = [\sum w(F_o^2 - F_c^2)^2/\sum w(F_o^2)^2]^{1/2}$ where $w = 1/\sigma^2(F_o^2) + (aP)^2 + bP$.

electron density difference map and its position and isotropic displacement parameters were refined. In addition, the MeOH hydrogen atom (also located and refined) is H-bonded to a chloride ligand of a neighboring complex in the crystal, with Cl···O(1S) = 3.13 Å. In the latter case, the relevant N(4A)···O-(7A) distance is 2.87 Å (hydrogen atom not located).

Spectroscopic Properties. The NMR or EPR spectral features observed for the Cu(I) and Cu(II) complexes in solution are in general accord with their structures determined by X-ray crystallography (see Supporting Information). The ^{1}H NMR spectra of the Cu(I) complexes exhibit an increase in the number and multiplicity of the macrocycle backbone methylene resonances compared to those of the free ligands, which is indicative of metal ion binding.[19a] Axial signals are observed in the X-band EPR spectra of the Cu(II) complexes, consistent with a $d_{x^2-y^2}$ ground state and square pyramidal geometries ($g_{\|} > g_{\perp} > 2.0$, $A_{\|} \sim 150-160$ G).

Infrared spectroscopy was found to be a useful tool for elucidating structural features of the various ligands and complexes, in particular for distinguishing the secondary and tertiary amides, identifying hydrogen-bonding interactions, and discerning if the amide carbonyl is bound to copper (Table 3). Spectra of the neat free ligands comprising secondary amides, L^{HAmH} (entry 1), L^{MeAmH} (entry 3), and L^{Piv} (entry 5), generally exhibit broad features in the N−H region (∼3300 cm^{-1}) consistent with the presence of multiple hydrogen bonds (presumably intra- and/or intermolecular, involving the amides and/or the macrocycle amine nitrogen atoms). These features are absent in spectra of the ligands L^{MeAmMe} and L^{HAmMe} (entries 2 and 4), which have tertiary amide groups. Features in the N−H region are also apparent in spectra of the copper complexes of the secondary amide ligands (collected as dilute KBr pellets, thus yielding peaks generally sharper than those for the free ligands), but observed differences in line shape and energy of the absorptions reflect divergent H-bonding to counterions or solvate molecules in the various compounds. Thus, as shown in Figure 3, little if any H-bonding is indicated by the appearance of sharp peaks at relatively high energy for the Cu(I) complexes of L^{HAmH} and L^{MeAmH} with PF_6^- and SbF_6^- counterions, respectively (upper two spectra). In contrast, significant broadening (by >2 × fwhm) and shifting to lower energy of the N−H features in the lower two cases, $[L^{Piv}Cu(CH_3CN)]O_3SCF_3$ and $[L^{HAmH}Cu(CH_3CN)]ClO_4$, are consistent with N−H···O interactions involving their respective counterions, which for the former was characterized by X-ray crystallography (vide supra). A broad N−H feature and multiple, broad O−H bands are present in the spectrum of $[L^{MeAmH}CuCl]PF_6\cdot$MeOH (not shown), consistent with the H-bonding involving the MeOH solvate that was identified in its X-ray structure. Not surprisingly, these H-bonding interactions are not evident in solution, as illustrated by FTIR data collected on $[L^{HAmH}Cu(CH_3CN)]ClO_4$ and $[L^{MeAmH}CuCl]PF_6\cdot$MeOH in CH_3CN and $CHCl_3$, respectively. For both, the broadened N−H features seen in KBr spectra are replaced by a sharp band at 3376 cm^{-1} in solution (∼60 mM), consistent with disrupton of the H-bonding between the amide N−H and the counterion and/or MeOH solvate.

Coordination of the amide carbonyl to the metal ion in complexes of the various ligands may be discerned readily from the position of the intense, sharp C−O stretching (amide I) vibration, which shifts ∼50 cm^{-1} lower when the amide is bound compared to when it is not (cf. pairs of entries 8/14 and 9/15 in Table 3). The secondary and tertiary amide ligands also may be differentiated by their amide I bands (2° bands being 20−30 cm^{-1} higher than 3°) and by the presence and absence, respectively, of lower energy features in the range 1510−1550 cm^{-1} ("amide II" bands arising from coupling of N−H bending and C−N stretching modes).[21] Amide carbonyl coordination is retained in solution, as evidenced by FTIR data for $[L^{MeAmH}CuCl]PF_6\cdot$MeOH in $CHCl_3$, which showed an amide I band at an energy identical to that observed in the KBr spectrum.

Finally, comparison of the carbonyl vibrational bands of the CO adducts of the Cu(I) complexes of L^{MeAmH} and L^{MeAmMe}

(21) Silverstein, R. M.; Bassler, G. C.; Morrill, T. C. *Spectrometric Identification of Organic Compounds*, 4th ed.; John Wiley & Sons: New York, 1981; p 126.

Table 2. Selected Bond Lengths (Å) and Angles (deg) for Complexes Characterized by X-ray Crystallography[a]

	$[L^{HAmMe}Cu(CH_3CN)]ClO_4$		
Cu(1)−N(1)	2.201(3)	Cu(1)−N(2)	2.158(3)
Cu(1)−N(3)	2.089(3)	Cu(1)−N(5)	1.869(3)
N(5)−Cu(1)−N(1)	117.05(13)	N(5)−Cu(1)−N(2)	129.79(14)
N(5)−Cu(1)−N(3)	136.7(2)	N(3)−Cu(1)−N(1)	86.00(12)
N(3)−Cu(1)−N(2)	85.91(13)	N(1)−Cu(1)−N(2)	84.22(12)
	$[L^{Piv}Cu(CH_3CN)]O_3SCF_3$		
	Molecule 1		
Cu(1)−N(1)	2.147(5)	Cu(1)−N(2)	2.150(5)
Cu(1)−N(3)	2.125(5)	Cu(1)−N(5)	1.858(6)
N(5)−Cu(1)−N(1)	128.2(2)	N(5)−Cu(1)−N(2)	124.3(2)
N(5)−Cu(1)−N(3)	132.6(2)	N(3)−Cu(1)−N(1)	85.5(2)
N(3)−Cu(1)−N(2)	86.4(2)	N(1)−Cu(1)−N(2)	84.3(2)
	Molecule 2		
Cu(1A)−N(1A)	2.164(4)	Cu(1A)−N(2A)	2.138(4)
Cu(1A)−N(3A)	2.139(4)	Cu(1A)−N(5A)	1.867(5)
N(5A)−Cu(1A)−N(1A)	120.7(2)	N(5A)−Cu(1A)−N(2A)	127.6(2)
N(5A)−Cu(1A)−N(3A)	135.6(2)	N(3A)−Cu(1A)−N(1A)	86.0(2)
N(3A)−Cu(1A)−N(2A)	86.0(2)	N(1A)−Cu(1A)−N(2A)	85.1(2)
	$[L^{HAmMe}CuCl]ClO_4$		
Cu(1)−O(1)	1.983(2)	Cu(1)−Cl(1)	2.2403(9)
Cu(1)−N(1)	2.045(3)	Cu(1)−N(2)	2.226(3)
Cu(1)−N(3)	2.092(3)	O(1)−C(14)	1.257(4)
O(1)−Cu(1)−N(1)	81.05(11)	O(1)−Cu(1)−N(2)	115.26(11)
N(1)−Cu(1)−N(2)	84.44(11)	O(1)−Cu(1)−N(3)	152.19(12)
N(3)−Cu(1)−N(2)	86.71(11)	N(1)−Cu(1)−N(3)	84.64(12)
N(1)−Cu(1)−Cl(1)	173.77(9)	O(1)−Cu(1)−Cl(1)	92.72(8)
N(3)−Cu(1)−Cl(1)	101.19(9)	N(2)−Cu(1)−Cl(1)	98.02(8)
	$[L^{MeAmH}CuCl]PF_6\cdot MeOH$		
Cu(1)−O(1)	2.012(2)	Cu(1)−Cl(1)	2.2575(9)
Cu(1)−N(1)	2.032(3)	Cu(1)−N(2)	2.225(3)
Cu(1)−N(3)	2.081(3)	O(1)−C(15)	1.259(4)
O(1)−Cu(1)−N(1)	81.82(10)	O(1)−Cu(1)−N(2)	114.44(10)
N(1)−Cu(1)−N(2)	85.10(10)	O(1)−Cu(1)−N(3)	153.73(10)
N(3)−Cu(1)−N(2)	86.71(11)	N(1)−Cu(1)−N(3)	84.88(11)
N(1)−Cu(1)−Cl(1)	173.20(8)	O(1)−Cu(1)−Cl(1)	91.79(7)
N(3)−Cu(1)−Cl(1)	101.92(8)	N(2)−Cu(1)−Cl(1)	95.50(7)
	$[L^{Piv}Cu(O_3SCF_3)]O_3SCF_3$		
Cu(1)−O(1)	1.967(2)	Cu(1)−O(2)	2.012(2)
Cu(1)−N(1)	2.042(3)	Cu(1)−N(2)	2.062(3)
Cu(1)−N(3)	2.215(3)	O(2)−S(1)	1.470(2)
O(1)−Cu(1)−N(1)	94.48(10)	O(1)−Cu(1)−O(2)	88.93(10)
O(1)−Cu(1)−N(2)	179.02(10)	O(2)−Cu(1)−N(1)	161.19(11)
O(2)−Cu(1)−N(3)	111.45(10)	O(2)−Cu(1)−N(2)	90.44(10)
N(3)−Cu(1)−N(2)	86.81(11)	N(1)−Cu(1)−N(2)	86.36(11)
O(1)−Cu(1)−N(3)	92.74(10)	N(1)−Cu(1)−N(3)	86.90(11)

[a] Estimated standard deviations indicated in parentheses.

(entries 12 and 13, Table 3) to those previously reported for like complexes of L^{iPr_3}, L^{iPr_2Bn}, and L^{Bn_3} (ν_{CO} = 2067, 2069, and 2084 cm^{-1}, respectively)[22] yields important information on the influences of the macrocycle substituents on the electron density at the bound copper ion. The trend in ν_{CO} values L^{MeAmH} > $L^{MeAmMe} \sim L^{Bn_3}$ > $L^{iPr2Bn} \sim L^{iPr3}$ indicates that the amide groups are electron withdrawing relative to the isopropyl and benzyl appendages.[23] In addition, the lower ν_{CO} for the complex of L^{MeAmMe} compared to that for the L^{MeAmH} case shows that amide N-alkylation, despite being at a relatively remote position, noticeably increases the amount of electron density at the metal.

We attempted to corroborate these conclusions about electronic effects of the amide-appended ligands that are based on analysis of FTIR data for the Cu(I)−carbonyl compounds by analyzing electrochemical data for $[LCu(CH_3CN)]^+$ (L = L^{MeAmH} and L^{MeAmMe}). Cyclic voltammograms of the complexes in CH_3CN with Bu_4NPF_6 (0.4 M) showed oxidation waves at 520 and 310 mV versus SCE, respectively, but worthwhile comparisons to other systems were prevented by the fact that the cyclic voltammetric responses were irreversible at all scan rates (0.05−1.0 V s^{-1}; no return reduction wave observed). Guided by the X-ray structural and FTIR spectral results, we speculate that the irreversible behavior arises from a drastic geometry change upon oxidation involving amide carbonyl coordination (i.e., conversion of a structure in Figure 1 to one like those shown in Figure 2).

Conclusions

In work that provides a foundation for future reactivity studies, we have synthesized and characterized a set of Cu(I) and Cu(II) complexes of new TACN ligands that contain a single amide arm. X-ray crystallographic and FTIR spectral studies showed that the amide group binds to the metal in the 5-coordinate square pyramidal Cu(II) compounds but remains unbound in the 4-coordinate Cu(I) species. These studies also showed that the secondary amides participate in intermolecular H-bonding to counterions and/or solvate molecules in the solid state. The amide-containing ligands are electron withdrawing relative to their isopropyl- or benzyl-substituted counterparts, as indicated by ν_{CO} values of Cu(I)−carbon monoxide adducts.

We have found that the attributes of these ligands have important implications in ongoing research on Cu(I)−dioxygen reactivity.[16] For example, the stabilities of bis(μ-oxo)dicopper compounds resulting from oxygenation of Cu(I) complexes of $L^{HAmRn'}$ and the resonance Raman spectral properties of (μ-η^2:η^2-peroxo)dicopper complexes of $L^{MeAmR'}$ are influenced by the nature of R′ (H or Me). We also have observed differences compared to simple alkylated cases in the pathways followed in the subsequent oxidative degradations of the amide ligands in the Cu(I)/O_2 reaction products. Guided by the fundamental work described herein, we hope to discern whether these effects are manifestations of amide carbonyl coordination, H-bonding, electronic influences, and/or some other property, with the ultimate goal of better understanding related issues in biology.

Experimental Section

General Procedures. All reagents and solvents were obtained from commercial sources and used as received unless noted otherwise. Solvents were dried according to published procedures[24] and distilled under N_2 immediately prior to use. Air-sensitive reactions were performed either in a Vacuum Atmospheres inert-atmosophere glovebox under a N_2 atmosphere or by using standard Schlenk and vacuum-line techniques. Methods used for physical characterization were as prevously described.[22] Optical absorption data between 800 and 1100 nm were collected on an HP 8453 diode array spectrophotometer, courtesy of Professor Lawrence Que, Jr. ^1H and $^{13}C\{^1H\}$ NMR data for ligands and copper(I) complexes, as well as the procedures used to prepare the various *N*-*tert*-butyl-*N*-R′-2-haloacetamides or -propionamides are provided in the Supporting Information. A published procedure was used to prepare 1,4-diisopropyl-1,4,7-triazacyclononane (L^H).[22,25]

(22) Mahapatra, S.; Halfen, J. A.; Wilkinson, E. C.; Pan, G.; Wang, X.; Young, V. G., Jr.; Cramer, C. J.; Que, L., Jr.; Tolman, W. B. *J. Am. Chem. Soc.* **1996**, *118*, 11555−11574.

(23) Dias, R. H. V.; Kim, H.-J.; Lu, H.-L.; Rajeshwar, K.; de Tacconi, N. R.; Derecskei-Kovacs, A.; Marynick, D. S. *Organometallics* **1996**, *15*, 2994−3003 and references therein.

(24) Perrin, D. D.; Armarego, W. L. F. *Purification of Laboratory Chemicals*; Pergamon Press: New York, 1988.

(25) Houser, R. P.; Halfen, J. A.; Young, V. G., Jr.; Blackburn, N. J.; Tolman, W. B. *J. Am. Chem. Soc.* **1995**, *117*, 10745−10746.

Table 3. Selected FTIR Data (cm^{-1}) for Amide-Appended TACN Ligands and Copper Complexes[a]

entry	complex	ν_{N-H}	$\nu_{amide\ I}$	$\nu_{amide\ II}$	ν_{X}[b]	$\nu_{C\equiv O}$
1	L^{HAmH}	3300 (br)	1671	1523		
2	L^{HAmMe}		1651			
3	L^{MeAmH}	3300 (br)	1667	1509		
4	L^{MeAmMe}		1652			
5	L^{Piv}	3360 (br)	1650	1529		
6	$[L^{HAmH}Cu(CH_3CN)]ClO_4$	3356	1671	1539	1096, 624	
7	$[L^{HAmH}Cu(CH_3CN)]PF_6$	3410	1671	1540	843	
8	$[L^{HAmMe}Cu(CH_3CN)]ClO_4$		1651		1091, 624	
9	$[L^{MeAmH}Cu(CH_3CN)]SbF_6$	3407	1677	1527	661	
10	$[L^{MeAmMe}Cu(CH_3CN)]SbF_6$		1644		660	
11	$[L^{Piv}Cu(CH_3CN)]O_3SCF_3$	3380	1648	1534	1275, 1262, 1155, 1033, 638	
12	$[L^{MeAmH}Cu(CO)]SbF_6$	3400	1674	1532	660	2092
13	$[L^{MeAmMe}Cu(CO)]SbF_6$		1645		660	2080
14	$[L^{HAmMe}CuCl]ClO_4 \cdot H_2O$	3470 (br)[c]	1600		1088, 652	
15	$[L^{MeAmH}CuCl]PF_6 \cdot MeOH$	3420 (br)[d]	1622	*e*	844, 559	
		3240 (br)				
		3080 (br)				
16	$[L^{Piv}Cu(O_3SCF_3)]O_3SCF_3$	3300 (br)	1594	*e*	1282, 1249, 1233, 1204, 1179, 1158, 1029, 1018, 638	

[a] FTIR spectra of ligands were collected on neat samples between NaCl plates; spectra of copper complexes were collected as dilute KBr pellets. [b] Stretching vibration(s) of counterion. [c] O−H stretching vibration (H_2O). [d] Multiple broad bands associated with ν_{N-H} of the amide and ν_{O-H} of the hydrogen-bonded methanol molecule. [e] A distinct amide II band is not observed, presumably due to overlap with the amide I band.

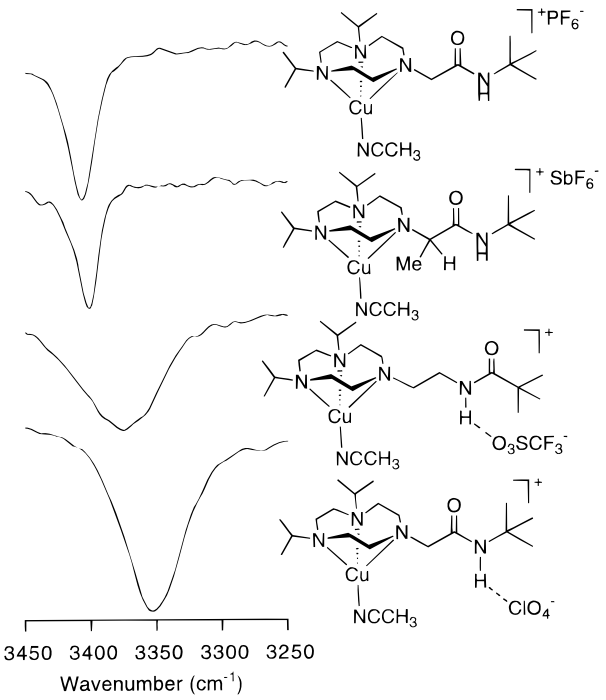

Figure 3. Amide N−H region of FTIR spectra of $[L^{RAmR'}Cu(CH_3CN)]X$ (R = H or Me, R′ = H; X = PF_6, SbF_6, or ClO_4) and $[L^{Piv}Cu(CH_3CN)]O_3SCF_3$ complexes. All spectra were acquired on solid samples dispersed in KBr.

1,4-Diisopropyl-7-(*N*-*tert*-butylacetamido)-1,4,7-triazacyclononane (L^{HAmH}).[1a] To a solution of L^H (255 mg, 1.20 mmol) in CH_3CN (15 mL) were added *N*-*tert*-butyl-2-chloroacetamide (179 mg, 1.20 mmol), sodium carbonate (500 mg), and tetrabutylammonium bromide (2 mg). The resulting mixture was refluxed for 3 h. After the reaction mixture was cooled to room temperature, it was filtered, and the remaining solid was washed with CH_2Cl_2 (2 × 5 mL). The combined filtrates were dried (Na_2SO_4) and subsequently brought to dryness under vacuum, leaving a pale yellow oil (370 mg, 95%). Although generally suitable for metal complex preparations, the product may be further purified by Kugelrohr distillation (130−134 °C, 0.2 Torr). GC/MS: t_R 13.04 min; *m*/*z* (relative intensity) 326 (1, M^+), 228 (100). HREIMS, *m*/*z*: calcd for $C_{18}H_{38}N_4O$, 326.3045; found, 326.3043. Anal. Calcd for $C_{18}H_{38}N_4O$: C, 66.20; H, 11.74; N, 17.17. Found: C, 65.50; H, 11.74; N, 16.75.

1,4-Diisopropyl-7-(*N*-*tert*-butyl-*N*-methylacetamido)-1,4,7-triazacyclononane (L^{HAmMe}). To a solution of L^H (224 mg, 1.05 mmol) in CH_3CN (15 mL) were added *N*-methyl-*N*-*tert*-butyl-2-chloroacetamide (172 mg, 1.05 mmol), sodium carbonate (222 mg, 2.09 mmol), and tetrabutylammonium bromide (2 mg). The resulting mixture was heated at reflux for 1 h. Subsequent workup as described above for L^{HAmH} yielded the product as a pale yellow oil (286 mg, 80%) which could be used for complex preparations or further purified by Kugelrohr distillation (130−134 °C, 0.2 Torr). GC/MS: t_R 13.52 min; *m*/*z* (relative intensity) 340 (1, M^+), 127 (100). HREIMS, *m*/*z*: calcd for $C_{19}H_{40}N_4O$, 340.3201; found, 340.3202. Anal. Calcd for $C_{19}H_{40}N_4O$: C, 66.00; H, 11.85; N, 16.46. Found: C, 66.13; H, 11.58; N, 16.02.

1,4-Diisopropyl-7-(*N*-*tert*-butyl-2-propionamido)-1,4,7-triazacyclononane (L^{MeAmH}). To a solution of L^H (476 mg, 2.24 mmol) in CH_3CN (20 mL) were added *N*-*tert*-butyl-2-bromopropionamide (496 mg, 2.39 mmol), Na_2CO_3 (475 mg, 4.48 mmol), and tetrabutylammonium bromide (∼3 mg). The resulting solution was heated at reflux for 1 h. The reaction mixture was cooled to ambient temperature, added to 20 mL of aqueous NaOH, and extracted with CH_2Cl_2 (2 × 60 mL). Following treatment with Na_2SO_4, the solution was brought to dryness under reduced pressure. Kugelrohr distillation (119−127 °C, 0.1 Torr) yielded the product as a thick clear oil (556 mg, 73%). HREIMS, *m*/*z*: calcd for $C_{19}H_{40}N_4O$, 340.3201; found, 340.3213. Anal. Calcd for $C_{19}H_{40}N_4O$: C, 66.00; H, 11.85; N, 16.46. Found: C, 65.83; H, 11.71; N, 16.12.

1,4-Diisopropyl-7-(*N*-methyl-*N*-*tert*-butyl-2-propionamido)-1,4,7-triazacyclononane (L^{MeAmMe}). To a solution of L^H (298 mg, 1.40 mmol) in CH_3CN (20 mL) were added *N*-methyl-*N*-*tert*-butyl-2-bromopropionamide (308 mg, 1.39 mmol), Na_2CO_3 (271 mg, 2.56 mmol), and tetrabutylammonium bromide (∼3 mg). The resulting solution was refluxed for 1 h and worked up as described above for L^{MeAmH}. Kugelrohr distillation (120−124 °C, 0.1 Torr) of the oily product yielded a thick clear oil (412 mg, 83%). HREIMS, *m*/*z*: calcd for $C_{20}H_{42}N_4O$, 354.3358; found, 354.3361. Anal. Calcd for $C_{20}H_{42}N_4O$: C, 67.73; H, 11.95; N, 15.81. Found: C, 66.96; H, 11.81; N, 15.77.

1,4-Diisopropyl-7-cyanomethyl-1,4,7-triazacyclononane (L^{CH_2CN}). To a solution of L^H (449 mg, 2.11 mmol) in CH_3CN (15 mL) was added chloroacetonitrile (140 mL, 2.21 mmol). After addition of Na_2CO_3 (0.750 g) and tetrabutylammonium bromide (5 mg), the resulting mixture was heated at reflux under nitrogen for 3 h. The resulting yellow-orange solution was cooled to room temperature and washed with 1 M NaOH (25 mL), the aqueous layer was washed with CH_2Cl_2 (2 × 30 mL), and the combined organic extracts were dried (Na_2SO_4). Removal of solvent under reduced pressure yielded the desired product as a yellow-orange oil (0.486 g, 91%). ^1H NMR ($CDCl_3$, 500 MHz): δ 3.35 (s, 2H), 2.85 (m, 6H), 2.68 (m, 4H), 2.53 (s, 4H), 0.95 (d, *J* =

6.6 Hz, 12H) ppm. $^{13}C\{^1H\}$ NMR ($CDCl_3$, 125 MHz): δ 116.9, 55.6, 54.5, 52.7, 51.7, 46.7, 18.2 ppm. FTIR (neat, cm^{-1}): 2232 (ν_{CN}). GC/MS: t_R 11.18 min; *m*/*z* (relative intensity) 252 (1, M^+), 154 (100). HREIMS, *m*/*z*: calcd for $C_{14}H_{28}N_4$, 252.2314; found, 252.2307.

1,4-Diisopropyl-7-(2-aminoethyl)-1,4,7-triazacyclononane ($L^{(CH_2)_2NH_2}$). L^{CH_2CN} (1.09 g, 4.31×10^{-3} mol) was dissolved in 1 M BH_3·THF (30 mL) and the resulting solution heated at reflux for 18 h. The clear solution was then cooled to room temperature, and ethanol was carefully added dropwise with vigorous stirring to destroy excess borane reagent. The solvent was then removed in vacuo. The resulting white solid was redissolved in 4 M HCl in methanol (30 mL). This acidic solution was heated at reflux for 2 h. Following cooling of the reaction mixture to ambient temperature, the methanol was removed in vacuo. The remaining aqueous solution was adjusted to pH >11 by addition of aqueous NaOH, extracted with CH_2Cl_2 (3 × 40 mL), and the combined extracts were dried with Na_2SO_4. Removal of the solvent under reduced pressure yielded the product as a faint yellow oil (872 mg, 79%). ^1H NMR ($CDCl_3$, 500 MHz): δ 2.85 (heptet, J = 6.6 Hz, 2H), 2.76 (m, 4H), 2.71 (t, J = 6.0 Hz, 2H), 2.65 (m, 4H), 2.57 (s, 4H), 2.56 (t, J = 6.0 Hz, 2H), 0.95 (d, J = 6.6 Hz, 12H) ppm. $^{13}C\{^1H\}$ NMR ($CDCl_3$, 125 MHz): δ 61.2, 56.4, 54.6, 53.0, 52.3, 40.3, 18.4 ppm. FTIR (neat, cm^{-1}): 3350 (N−H, br). HREIMS, *m*/*z*: calcd for $C_{14}H_{32}N_4$, 256.2627; found, 256.2628.

1,4-Diisopropyl-7-(2-pivalamidoethyl)-1,4,7-triazacyclononane (L^{Piv}). To a solution of $L^{(CH_2)_2NH_2}$ (824 mg, 3.22 mmol) in CH_2Cl_2 (15 mL) were added NEt_3 (580 mL, 4.18 mmol) and trimethylacetyl chloride (436 mL, 3.54 mmol). The resulting solution was stirred at room temperature for 24 h. The CH_2Cl_2 solution was then washed with water (3 × 40 mL), the combined water extracts were adjusted to pH ∼9 by addition of aqueous NaOH, and the basic solution was then extracted with CH_2Cl_2 (4 × 50 mL). The combined CH_2Cl_2 fractions were dried (Na_2SO_4), and the CH_2Cl_2 was removed in vacuo to yield the product as a pale yellow oil (590 mg, 54%). GC/MS: t_R 13.88 min; *m*/*z* (relative intensity) 340 (1, M^+), 128 (100). Anal. Calcd for $C_{19}H_{40}N_4O$: C, 66.00; H, 11.85; N, 16.46. Found: C, 64.79; H, 11.49; N, 15.76.

[L^{HAmH}Cu(CH_3CN)]X (X = ClO_4^- or PF_6^-). To a solution of L^{HAmH} (83 mg, 0.26 mmol) in CH_3CN (2 mL) was added solid [Cu(CH_3CN)$_4$]ClO_4 (83 mg, 0.25 mmol). The mixture was stirred at room temperature until all of the Cu(I) starting material had dissolved (∼10 min). The clear solution was then added to Et_2O (15 mL), which resulted in the immediate precipitation of a white solid. Additional material precipitated after allowing the solution to stand at −20 °C overnight. Subsequent decantation of the solvent and drying of the remaining solid under a stream of N_2 yielded the pure product (86 mg, 64%). A similar procedure was followed for the case X = PF_6^- (50% yield). Anal. Calcd for X = ClO_4^-, $C_{20}H_{41}N_5O_5CuCl$: C, 45.35; H, 7.81; N, 13.23. Found: C, 45.58; H, 7.54; N, 13.17. Calcd for X = PF_6^-, $C_{20}H_{41}N_5OCuPF_6$: C, 41.72; H, 7.18; N, 12.17. Found: C, 42.25; H, 7.23; N, 12.08.

[L^{HAmMe}Cu(CH_3CN)]ClO_4. To a solution of L^{HAmMe} (478 mg, 1.41 mmol) in CH_3CN (2 mL) was added [Cu(CH_3CN)]ClO_4 (412 mg, 1.26 mmol) over the course of 5 min. After the resulting solution was stirred for an additional 10 min, Et_2O (30 mL) was added, resulting in the formation of a cloudy solution. Cooling of the solution to −20 °C overnight resulted in the deposition of the product as white crystals (281 mg, 40%). Anal. Calcd for $C_{21}H_{43}N_5O_5CuCl$: C, 46.39; H, 7.98; N, 12.89. Found: C, 46.37; H, 7.86; N, 12.73.

[L^{MeAmH}Cu(CH_3CN)]SbF_6. To a CH_3CN solution (1 mL) of L^{MeAmH} (173 mg, 0.508 mmol) was added solid [Cu(CH_3CN)$_4$]SbF_6 (213 mg, 0.459 mmol). The resulting pale yellow solution was stirred for an additional 10 min and was then added to Et_2O (20 mL). The resulting cloudy solution was cooled to −20 °C overnight, which led to the deposition of the product as a white powder (206 mg, 66%). Anal. Calcd for $C_{21}H_{43}N_5OCuSbF_6$: C, 37.10; H, 6.38; N, 10.31. Found: C, 37.50; H, 6.36; N, 10.19.

[L^{MeAmMe}Cu(CH_3CN)]SbF_6. To a CH_3CN solution (1 mL) of L^{MeAmMe} (157 mg, 0.444 mmol) was added solid [Cu(CH_3CN)$_4$]SbF_6 (191 mg, 0.413 mmol), resulting in the formation of a pale yellow solution. Workup as above for [(L^{MeAmH})Cu(CH_3CN)]SbF_6 yielded the product as clear crystals (192 mg, 67%). Anal. Calcd for $C_{22}H_{45}N_5OCuSbF_6$: C, 38.09; H, 6.54; N, 10.10. Found: C, 37.51; H, 6.30; N, 10.10.

[L^{Piv}Cu(CH_3CN)]O_3SCF_3. To a solution of L^{Piv} (102 mg, 0.299 mmol) in CH_2Cl_2 (1 mL) was added a slurry of [Cu(CH_3CN)$_4$]O_3SCF_3 (101 mg, 0.269 mmol) in CH_2Cl_2 (0.5 mL), resulting in the formation of a yellow solution. After being stirred for 10 min at room temperature, the CH_2Cl_2 solution was added dropwise to Et_2O (20 mL). The resulting cloudy solution was allowed to stand at −20 °C for 16 h. A white microcrystalline solid was isolated after careful decantation of the remaining solvent and drying of the solid under vacuum (119 mg, 75%). Anal. Calcd for $C_{22}H_{43}N_5O_4SF_3Cu$: C, 44.50; H, 7.31; N, 11.80. Found: C, 44.56; H, 7.17; N, 11.66.

[L^{MeAmMe}Cu(CO)]SbF_6. Solid [L^{MeAmMe}Cu(CH_3CN)]SbF_6 (193 mg, 0.278 mmol) was dissolved in acetone (∼8 mL). Carbon monoxide was then bubbled through the solution for 1−2 min. The solvent was removed, and the remaining white solid was washed with Et_2O (10 mL), collected by filtration, and dried in vacuo (115 mg, 61%). Anal. Calcd for $C_{21}H_{42}N_4O_2CuSbF_6$: C, 37.05; H, 6.22; N, 8.24. Found: C, 37.08; H, 6.13; N, 8.18.

[L^{MeAmH}Cu(CO)]SbF_6. Solid [L^{MeAmH}Cu(CH_3CN)]SbF_6 (223 mg, 0.329 mmol) was dissolved in acetone (∼8 mL). Within approximately 1−2 min, oxidation of a portion of the starting material occurred, as indicated by development of a pale blue color. Carbon monoxide was bubbled through this solution for 1−2 min. Following removal of the solvent in vacuo, the crude solid was redissolved in acetone (1 mL), and the resulting pale blue solution was added to Et_2O (20 mL). Cooling of the cloudy solution at −20 °C for 1 h led to the deposition of a blue solid, which was removed by filtration. The clear, colorless filtrate was cooled at −20 °C for an additional 4 h, which led to the deposition of the product as a white microcrystalline solid (43 mg, 20%). Anal. Calcd for $C_{20}H_{40}N_4O_2CuSbF_6$: C, 36.03; H, 6.05; N, 8.41. Found: C, 35.21; H, 5.97; N, 8.14.

[L^{HAmMe}CuCl]ClO_4·H_2O. To a solution of L^{HAmMe} (61 mg, 0.18 mmol) in MeOH (2 mL) was added $CuCl_2$ (24 mg, 0.18 mmol), resulting in the formation of a green solution. Following stirring of the solution for 10 min, excess $NaClO_4$ was added, and the solution was placed in a −20 °C freezer overnight. A blue-green precipitate was removed by filtration. Recrystallization of the precipitate from vapor diffusion of Et_2O into a 1:1 MeOH/CH_2Cl_2 solution yielded the product as blue-green crystals (29.4 mg, 31%). ISP-MS (CH_2Cl_2), *m*/*z* (relative intensity): 502.1 ([M − Cl]$^+$, 100%), 438.2 ([M − ClO_4]$^+$, 60%). UV−vis (CH_2Cl_2) [λ_{max}, nm (ϵ, L mol^{-1} cm^{-1})]: 292 (6500), 714 (100), 806 (100). Anal. Calcd for $C_{19}H_{40}N_4O_5Cl_2Cu$·H_2O: C, 41.07; H, 7.62; N, 10.09. Found: C, 41.34; H, 7.11; N, 10.06.

[L^{MeAmH}CuCl]PF_6·MeOH. To a MeOH solution (1 mL) of L^{MeAmH} (376 mg, 1.11 mmol) was added solid $CuCl_2$ (149 mg, 1.11 mmol) to yield a green-blue solution after stirring for 10 min. Excess NH_4PF_6 (850 mg) was added, and the solution was cooled to −20 °C overnight. The resulting blue precipitate was recrystallized by diffusing Et_2O into a 1:1 CH_2Cl_2/methanol solution to yield the product as bright blue crystals (405 mg, 59%). UV−vis (CH_2Cl_2) [λ_{max}, nm (ϵ, L mol^{-1} cm^{-1})]: 294 (7000), 718 (100), 836 (100). ISP-MS (CH_2Cl_2), *m*/*z* (relative intensity): 548.2 ([M − Cl]$^+$, 15%), 438.0 ([M − PF_6]$^+$, 100%), 403.0 ([M − Cl − PF_6]$^+$, 35%). Anal. Calcd for $C_{19}H_{40}N_4OClCuPF_6$·CH_3OH: C, 39.01; H, 7.21; N, 9.10. Found: C, 38.77; H, 6.97; N, 9.02. The presence of MeOH in the analytical sample was corroborated by the X-ray crystal structure results.

[L^{Piv}Cu(O_3SCF_3)]O_3SCF_3. To a THF solution (5 mL) of L^{Piv} (109 mg, 0.321 mmol) was added solid $Cu(OTf)_2$ (115 mg, 0.319 mmol). The resulting green-blue solution was stirred overnight at ambient temperature. The volume of the solution was then reduced to 1 mL in vacuo, and pentane (5 mL) was added, resulting in the deposition of a blue-green precipitate. Recrystallization of the precipitate by Et_2O diffusion into a THF/CH_2Cl_2 (1:1) solution yielded blue-green block-shaped crystals suitable for single-crystal X-ray diffraction analysis (136 mg, 61%). UV−vis (CH_2Cl_2) [λ_{max}, nm (ϵ, L mol^{-1} cm^{-1})]: 302 (3800), 684 (100). ISP-MS (CH_2Cl_2), *m*/*z* (relative intensity): 552.2 ([M − OTf]$^+$, 100%). Anal. Calcd for $C_{21}H_{40}N_4O_7S_2F_6Cu$: C, 35.94; H, 5.75; N, 7.99. Found: C, 35.30; H, 5.64; N, 7.60.

X-ray Crystallography. Data Collection. A colorless block crystal of [L^{Piv}Cu(CH_3CN)]O_3SCF_3, a blue-green block crystal of [L^{Piv}Cu(O_3-

SCF_3)]O_3SCF_3, a colorless block crystal of [L^{HAmMe}Cu(CH_3CN)]ClO_4, a blue rhombic crystal of [L^{HAmMe}CuCl]ClO_4, and a blue plate crystal of [L^{MeAmH}CuCl]PF_6·MeOH were attached to a glass fiber with heavyweight oil and mounted on the Siemens SMART system for data collection at 173(2) K. Initial cell constants were calculated from reflections harvested from three sets of 20−30 frames. These initial sets of frames were oriented such that orthogonal wedges of reciprocal space were surveyed. This produced orientation matrixes determined from 50 to 300 reflections. Final cell constants were calculated from a set of strong reflections from the actual data collection. A hemisphere data collection technique was used whereby a randomly oriented region of reciprocal space was surveyed to the extent of 1.3 hemispheres to a resolution of 0.84 Å. Three major swaths of frames were collected with 0.30° steps in ω. The resulting highly redundant data provided good ψ input for a semiempirical absorption correction applied to data for each case. Additional crystal and refinement information is given in Table 1.

Structure Solution and Refinement. Space group determinations were made on the basis of systematic absences and intensity statistics. The structures were solved by direct methods which provided most non-hydrogen atoms from the *E* map. The remainder of the non-hydrogen atoms were located following several full-matrix least-squares/difference Fourier cycles. All non-hydrogen atoms were refined with anisotropic displacement parameters, and all hydrogen atoms were placed in ideal positions and were refined as riding atoms with individual isotropic displacement parameters unless indicated otherwise. Unique features of the structure solutions of individual complexes are given below.

[L^{Piv}Cu(CH_3CN)]O_3SCF_3. The asymmetric unit contains two independent formula units. One *tert*-butyl group was found to be disordered; a split-atom model was applied to account for the disorder. The occupancies of the two rotationally disordered groups are 0.423 (C(17A)−C(18A)−C(19A)) and 0.577 (C(17B)−C(18B)−C(19B)). The shortest intermolecular contacts involve hydrogen bonds between the triflate anions and the amide hydrogen atoms; these distances are O(4)···H(4AA) (2.043 Å) and O(3A)···H(4A) (2.276 Å).

[L^{HAmMe}Cu(CH_3CN)]ClO_4. The ClO_4^- anion was found to be disordered over two positions of occupancies 0.61 (O(2′)−O(3′)−O(4′)−O(5′)) and 0.40 (O(2)−O(3)−O(4)−O(5)); the position of the central chloride atom is common to both orientations. Bond length and angle constraints were applied to the ion, and the individual atomic displacement parameters were also constrained to approximate rigid-body motion.

[L^{MeAmH}CuCl]PF_6·MeOH. A methanol solvate molecule was located in the asymmetric unit. Both the methanol O−H proton and the amide proton were located from the difference map, and their positions and isotropic displacement parameters were refined. The methanol oxygen atom is hydrogen-bonded to the amide proton (O(1S)···H(1A2) = 1.980 Å, O(1S)···N(4) = 2.854 Å). Additionally, the methanol proton is hydrogen-bonded to the chloride ligand of a neighboring complex (Cl···H(1A1) = 2.355 Å, Cl···O(1S) = 3.127 Å). Thus, two cations are linked together in the unit cell by a methanol molecule. The PF_6^- anion is rotationally disordered about the F(5)−P(1)−F(6) axis; this was modeled with two sets of equatorial fluorides with occupancies of 0.81 (F(1)−F(2)−F(3)−F(4)) and 0.19 (F(1′)−F(2′)−F(3′)−F(4′)).

All calculations were performed using the SHELXTL-Plus V5.0 suite of programs on an SGI INDY R4400-SC computer.[26] Thermal ellipsoid drawings of the complexes appear in Figures 1 and 2, and selected bond lengths and angles for each are presented in Table 2. Full details of the structure determinations, including fractional atomic coordinates, full tables of bond lengths and angles, anisotropic displacement parameters, torsion angles, and hydrogen atom coordinates, are included in the Supporting Information.

Acknowledgment. We thank the NIH (Grant GM47365 to W.B.T. and a postdoctoral fellowship to L.M.B.), the NSF (NYI award to W.B.T.), the Camille & Henry Dreyfus Foundation (fellowship to W.B.T.), and Unilever Corp. for financial support of this work.

Supporting Information Available: Tables giving ^1H and ^{13}C-{^1H} NMR data for ligands and copper(I) complexes and text describing preparative procedures for the various *N*-*tert*-butyl-*N*-R′-2-haloacetamides or -propionamides used for the ligand syntheses (5 pages). X-ray crystallographic files, in CIF format, for the structure determinations are available on the Internet only. Ordering and access information is given on any current masthead page.

IC971115F

(26) *SHELXTL V5.0*; Siemens Energy & Automation, Inc.: Madison, WI.